Passive diastolic modelling of human ventricles: effects of base movement and geometrical heterogeneity

Authors: Arnab Palit[1,3], Pasquale Franciosa[1], Sunil K. Bhudia[2], Theodoros N. Arvanitis[3], Glen A. Turley[1], Mark A. Williams[1]

[1] *WMG, The University of Warwick, Coventry, UK*
[2] *University Hospitals Coventry and Warwickshire, Coventry, UK*
[3] *Institute of Digital Healthcare, WMG, The University of Warwick, Coventry, UK*

Corresponding Author: Arnab Palit
WMG,
University of Warwick,
Coventry,
CV4 7AL
Tel: +44 (0) 24 7615 1798
Fax: +44 (0) 24 7652 4307
Email : arnab.palit@warwick.ac.uk

Email address:
Arnab Palit - arnab.palit@warwick.ac.uk
Pasquale Franciosa - P.Franciosa@warwick.ac.uk
Sunil K. Bhudia - S.Bhudia@warwick.ac.uk
Theodoros N. Arvanitis - T.Arvanitis@warwick.ac.uk
Glen A. Turley - Glen.Turley@warwick.ac.uk
Mark A. Williams - M.A.Williams.1@warwick.ac.uk

Word count: 3996

Abstract:

Left-ventricular (LV) remodelling, associated with diastolic heart failure, is driven by an increase in myocardial stress. Therefore, normalisation of LV wall stress is the cornerstone of many therapeutic treatments. However, information regarding such regional stress-strain for human LV is still limited. Thus, the objectives of our study were to determine local diastolic stress-strain field in healthy LVs, and consequently, to identify the regional variations amongst them due to geometric heterogeneity. Effects of LV base movement on diastolic model predictions, which were ignored in the literature, were further explored. Personalised finite-element modelling of five normal human bi-ventricles was carried out using subject-specific myocardium properties. Model prediction was validated individually through comparison with end-diastolic volume and a new shape-volume based measurement of LV cavity, extracted from magnetic resonance imaging. Results indicated that incorporation of LV base movement improved the model predictions (shape-volume relevancy of LV cavity), and therefore, it should be considered in future studies. The LV endocardium always experienced higher fibre stress compared to the epicardium for all five subjects. The LV wall near base experienced higher stress compared to equatorial and apical locations. The lateral LV wall underwent greater stress distribution (fibre and sheet stress) compared to other three regions. In addition, normal ranges of different stress-strain components in different regions of LV wall were reported for five healthy ventricles. This information could be used as targets for future computational studies to optimise diastolic heart failure treatments or design new therapeutic interventions/devices.

Keywords: Ventricular diastolic mechanics, Finite element, Patient-specific modelling, Ventricular geometry, Fibre structure

1. Introduction:

Epidemiological studies reported that more than half of the patients diagnosed with heart failure (HF) have left-ventricular (LV) diastolic dysfunction with normal systolic pump function (Wang and Nagueh, 2009). LV remodelling process, associated with diastolic heart failure (HF), was identified to be driven by an increase in LV wall stress (Lee et al., 2014, Wall et al., 2006). The LV remodelling is, therefore, increasingly recognized as a potential target for therapeutic interventions, which include the use of hydrogel injection (Lee et al., 2013a), anisotropic reinforcement (Fomovsky et al., 2012), cardiac support and resistance devices (Lee et al., 2014, Wenk et al., 2013a). The main objective of these surgical interventions was to normalise the LV wall stress at end diastole (ED). Finite element (FE) modelling, in combination with new cardiac imaging modalities and advanced simulation tools, can be used to analyse the diastolic mechanics of healthy heart and identify the normal ranges of stress-strain distribution in LV wall. Such information will provide a greater insight of the physiology and pathophysiology of HF patients, and thereby, predict their response to medical and surgical interventions.

The majority of diastolic FE modelling in existing literature was based on either animal heart or idealised geometry of single LV (Guccione et al., 1995, Costa et al., 1996, Usyk et al., 2000, Vetter and McCulloch, 2000) (Table 1). With the advancement in imaging modalities over the years, subject-specific single LV geometry was used for FE modelling (Wang et al., 2013, Wang et al., 2009, Genet et al., 2014). Recent study by Palit et al. (2015b) showed that the right-ventricle (RV) deformation has a significant effect on LV wall stress distribution and should be considered during ventricular modelling. Furthermore, in majority of the computational models, Fung-type transversely isotropic constitutive law was used (Guccione et al., 1995, Costa et al., 1996, Vetter and McCulloch, 2000, Wang et al., 2009, Genet et al., 2014) (Table 1). In contrast, simple shear test of pig and human myocardium

(Dokos et al., 2002, Sommer et al., 2015b, Gultekin et al., 2016) clearly exhibited orthotropic viscoelastic behaviour. Modified Fung-type (Usyk et al., 2000, Costa et al., 2001) and pole-zero law (Stevens et al., 2003) were used in diastolic modelling to incorporate material orthotropy. However, the material parameters in these orthotropic models were merely used as weighting factors, rather than any physical significance (Göktepe et al., 2011). Recently, Holzapfel and Ogden (2009) developed a constitutive law that considered the locally orthotropic tissue architecture. The parameters of this model were closely related to the characteristic microstructure of myocardium. However, all the diastolic FE studies of human LV using Holzapfel-Ogden law used experimental data of animal myocardium which resulted in too stiff stress-strain relation, and thereby, unable to produce expected LV inflation through simulation (Wang et al., 2013, Palit et al., 2015b, Baillargeon et al., 2014). The majority of diastolic modelling of human LV used only one subject except the study conducted by Genet et al. (2014) which had limitations of using single LV model and transversely isotropic material law (Table 1). Therefore, the effect of geometrical heterogeneity in LV wall stress prediction is an important issue which is addressed in this study. There are two types of geometrical heterogeneity - (a) local geometrical heterogeneity which is present within a single LV geometry, and (b) global geometrical heterogeneity that is observed amongst different LV geometries (amongst different subjects). In this study, the focus was mainly on the global geometrical heterogeneity although local heterogeneity was included as the geometry was developed from subject-specific MRI.

In majority of the FE models, kinematic constraints were typically used to fix longitudinal basal movement to avoid any rigid body displacement and allowed the apex to move freely (Wang et al., 2013, Genet et al., 2014, Walker et al., 2008, Eriksson et al., 2013). However, as reported by Wang et al. (2009) and observed from CMRI data, the apex of the

heart did not move considerably during diastole, as opposed to the mitral valve plane (Figure 1c).

Therefore, in the present study, personalised passive diastolic modelling of five normal human BV was carried out to address the following objectives - (1) to identify the effect of LV base movement on FE model predictions; (2) to investigate the changes in LV wall stress-strain distribution at ED due to geometric heterogeneity; and (3) to provide a reference map of regional stress-strain field in healthy LV wall at ED.

2. Material and Methods

2.1 Construction of Subject-specific Bi-ventricular Geometry

ECG gated, breathe hold, steady state free precession (SSFP) cardiac magnetic resonance imaging (CMRI) was performed to capture the images of five normal human ventricles at UHCW, Coventry, UK. BSREC ethics approval and patient consents were obtained to carry out the research on anonymised human data. Details of the mesh geometry construction were described in (Palit et al. (2015b), Palit et al. (2014)). The early-diastolic volume (ErDV), EDV and ejection fraction (EF), were calculated from CMRI (Figure 1a). Average longitudinal movement of base and apex during diastole were measured from constructed LV cavity geometry (Figure 1b). It was observed that the average longitudinal movement of base was considerably higher than the movement of apex for all five ventricles during diastole (Figure 1c). Figure 2a, 2b and 2c show the early diastolic BV mesh geometries, early and end diastolic LV cavities respectively, constructed from CMRI. Detailed CMRI scanning protocol and demographic information of the subjects are enclosed in Appendix A.

2.2 Construction of Rule-based Fibre-Sheet Orientation

Myocardial fibre-sheet orientation was implemented by 'Laplace-Dirichlet-Region growing-FEM' (LDRF) based algorithm (Palit et al., 2014, Wong and Kuhl, 2014). Based on previous studies (Streeter et al., 1969, Arts et al., 2001, Rohmer et al., 2007, Sommer et al., 2015a, Holzapfel and Ogden, 2009), the fibre orientation was defined by a linear variation of helix angle from -70° in the sub-epicardium and RV septal endocardium to almost 0° in the mid-wall to +70° at sub-endocardium and RV free wall endocardium for all five ventricles (Figure 2d). The sheet direction was assumed to be aligned with local radial direction as it has very little effect on passive stress-strain distribution of LV wall (Wang et al., 2013).

2.3 Constitutive Law for Passive Myocardium

The Holzapfel-Ogden material law (Eq. (1)) was used to define myocardium (Holzapfel and Ogden, 2009). Appendix B includes a detailed description of the strain energy function. Table 2 shows the material parameters used in this study. A brief description of the material parameter identification is included in Appendix C.

$$\Psi = K\left(\frac{J^2-1}{2}-\ln J\right)+\frac{a}{2b}\exp\left[b(\bar{I}_1-3)\right] + \sum_{i=f,s}\frac{a_i}{2b_i}\left\{\exp\left[b_i(\bar{I}_{4i}-1)^2\right]-1\right\}+\frac{a_{fs}}{2b_{fs}}\left\{\exp\left[b_{fs}(\bar{I}_{8fs})^2\right]-1\right\} \quad (1)$$

2.4 Finite Element Model of Passive LV Mechanics

Early-diastolic (ErD) BV mesh geometry was constructed from ErD CMRI of human ventricle. According to state-of-the-art, ErD is assumed as initial stress free configuration since the ventricular pressure is lowest at this point, and therefore, stress is minimum (Usyk et al., 2000, Genet et al., 2014, Palit et al., 2015b, Sun et al., 2009, Wenk et al., 2011b, Wenk et al., 2011a, Palit et al., 2015a). Due to the unavailability of subject-specific ventricular

pressure, which requires invasive measurement, LV EDP was considered $10\ mmHg$ (Genet et al., 2014, Wang et al., 2013, Lee et al., 2013b, Lee et al., 2013a). One third of the LV blood pressure was applied on the RV endocardium (Palit et al., 2015b). Traditionally, the longitudinal movement of the base and the circumferential displacement of epicardial wall at the base were suppressed whereas apex was set free (Lee et al., 2014, Wang et al., 2013, Genet et al., 2014, Palit et al., 2015b, Eriksson et al., 2013, Wenk et al., 2011b, Dorri, 2004). However, as reported by Wang et al. (2009) and observed from CMRI (Figure 1b and c), the upward basal movement was greater compared to the movement of apex during diastole. Therefore, two cases were considered for all five BVs to explore the effect of base movement. Case-1 used the traditional method of constraining the longitudinal movement of base and allowing the apex to move free (Lee et al., 2014, Wang et al., 2013, Genet et al., 2014, Palit et al., 2015b, Eriksson et al., 2013, Dorri, 2004, Wenk et al., 2011b). In case-1, the circumferential displacement of epicardial wall at the base is also constrained along with the longitudinal movement of base as described in Sun et al. (2009), Wenk et al. (2013a), and Wang et al. (2013). Case-2 followed the method of Wang et al. (2009) in order to include the base movement to match the data from the CMRI. Average longitudinal displacement (Figure 1c) was prescribed in all the basal nodes except the basal endocardial nodes (Wang et al., 2009). The movement of apex and the circumferential displacement of epicardial wall at base was supressed in order to avoid any rigid body displacement (Wang et al., 2009). Radial direction was assumed to be free to deform (Wang et al., 2013, Wenk et al., 2013a) for both cases.

In order to study the stress-strain distribution of the LV wall, three short-axis slices were considered: (1) basal slice positioned $10\,mm$ below the base; (2) equatorial slice located $20\,mm$ below the basal slice; and (3) apical slice positioned $20\,mm$ above the apex. In addition, two long-axis slices were defined. The *s-l* slice, passing through the septum and

lateral wall, divided both RV and LV in the middle. The *a-p* slice, passing through anterior and posterior wall, divided the LV cavity in the middle. In addition, each short-axis location was divided in four regions such as: anterior, lateral, posterior, and septum.

3. Results

3.1 Model Validation:

Validation of Holzapfel-Ogden material model implementation in FE framework was detailed in Palit (2015). A shape-volume based validation procedure was introduced, for the first time, instead of comparing only LV EDV. The geometry of LV cavity at ED, constructed from CMRI, was attributed as 'original' shape (Figure 2c). The geometry of LV cavity at ED, resulted from simulation, was considered as 'predicted' shape. The intersected volume between 'original' and 'predicted' geometry was calculated to incorporate shape-volume relevancy (Figure 3b), and consequently, to check the accuracy of the model predictions. This is performed in 3-matic by importing both the .stl files of 'original' and 'predicted' LV cavity, and thereafter, by using the intersected volume option. Figure 3c shows that the 'predicted' LV cavity is able to produce $85.91 \pm 2.84\%$ shape-volume similarities when compared with 'original' LV cavity at ED (case-2).

3.2 Effect of Base Movement

Two separate simulations (case-1 and case-2) were carried out for each BV to investigate the effect of base movement on FE model prediction. Three different parameters were compared. First, the LV EDV was compared by plotting the LV end diastolic pressure volume relation (EDPVR) for both the cases (Figure 3a). It was observed that the base movement did not affect the EDPVR of LVs, and therefore, both cases achieved same LV EDV as measured from CMRI. Second, although both the cases produced same LV EDPVR,

198 the shape-volume relevancy was better for case-2 for all subjects ($85.91 \pm 2.84\%$ in case-2
199 compared to $70.72 \pm 4.05\%$ in case-1) (Figure 3c). Third, a qualitative comparison in fibre
200 stress-strain distribution in LV wall (BV1) at ED for both cases was carried out (Figure 4). It
201 was identified that the following areas experienced higher fibre stress in case-2: anterior and
202 posterior regions of basal and equatorial locations, LV endocardium and near epicardium.
203 The fibre stress distribution at apical location was completely different between the cases
204 (Figure 4). Moreover, the entire LV wall experienced higher fibre strain in case-2.

205 **3.3 Stress-strain amongst the different wall locations of the five ventricles**

206 Figure 5 shows that the LV endocardium experiences higher fibre stress compared to
207 the LV epicardium. The average fibre stress was marginally higher in the equatorial location
208 compared to the basal and the apical location (except for BV3). Both sheet and sheet-normal
209 stresses were greater in the basal location and minimal in the apical location for all five
210 ventricles (Figure 6b). Variations in fibre and sheet stresses in the apical location were higher
211 in comparison with the other locations (Figure 6a). In contrast, the variation in sheet-normal
212 stress was greater in the basal location. The average fibre stress at ED was higher compared
213 to sheet and sheet-normal stresses. The ranges of fibre, sheet and sheet-normal stresses were
214 approximately in the range of 0 to 6 *kPa*, -1.5 to $+1.5$ *kPa and* -1 to $+5$ *kPa*
215 respectively for all locations (Figure 6a).

216 Figure 6c and 6d show the average GL strain in local cardiac coordinate ($\mathbf{e_c}, \mathbf{e_z}, \mathbf{e_n}$)
217 (Palit et al., 2014, Wang et al., 2013). The circumferential and radial strains were higher in
218 the basal and the equatorial locations compared to the apical location, whereas the
219 longitudinal strain was higher in the apical location and lowest in the equatorial location. The
220 circumferential GL strain was greater in comparison with longitudinal and radial strain
221 (Figure 6c).

3.4 Stress-strain amongst the different wall regions of the five ventricles

The lateral region of LV in all the short-axis locations was experienced comparatively higher fibre stress for all the ventricles (except BV4 in equatorial location) whereas the septum in the apical location experienced lower fibre-stress (Figure 7b). Compressive sheet stress was greater in the lateral region of the equatorial and the apical locations. Sheet-normal stress was higher in the posterior region of the equatorial location whereas the lateral wall experienced comparatively lower sheet-normal stresses (except BV3 sheet-normal stress). Moreover, the variation in fibre-stress amongst the regions was less in the basal and the equatorial locations compared to the variation in the apical location. The ranges of stresses, experienced by different regions of LV wall in different short-axis location, are shown in Figure 7a.

The ranges of different GL strain components are plotted in Figure 8a. High circumferential GL strain was experienced by the lateral wall at the basal location, and the posterior region of the equatorial and the apical locations (Figure 8b). The anterior and the septum wall received comparatively lower circumferential GL strain. The longitudinal GL strain was less in the posterior region of the basal and the equatorial locations.

4. Discussion

4.1 Comparison with state-of-the-art

Passive diastolic modelling was carried out for five human ventricles to investigate the effect of base movement and geometrical heterogeneity on LV wall stress-strain distributions. Authors' previous work (Palit et al., 2015b) included the effect of fibre orientation and right ventricle (RV) on LV mechanics using porcine myocardium data, and

without considering base movement. The current study aimed to explore the effect of global geometrical heterogeneity and base movement on LV mechanics using human myocardium properties. The previous study was conducted by implementing different fibre orientation on single ventricular geometry, whereas in this study, five BV geometries were used with similar fibre structure to find the effect of global geometrical heterogeneity. Several improvements were incorporated in the present study over state-of-the-art for better model prediction. Firstly, BV geometries were used in the study to consider the effect of RV deformation. Palit et al. (2015b) reported that the inclusion of RV deformation in computational model not only changed the stress-strain distribution pattern but also increased LV wall stress-strain during diastole. The majority of previous studies used only single LV geometry (Genet et al., 2014, Wang et al., 2013, Wang et al., 2009), and therefore, the effects of RV deformation were not considered. Secondly, subject-specific passive orthotropic material properties for human myocardium were used instead of transversely isotropic properties (Genet et al., 2014). Thirdly, LV base movement was included in diastole to predict more accurate shape-volume changes of ventricles during diastole. Although Wang et al. (2009) included base movement in their model, the effect was first investigated in this study. Fourthly, a new shape-volume based validation procedure was introduced to measure the model prediction accuracy. Finally, the variation of fibre, sheet and sheet-normal stresses (and strains) amongst different wall regions and locations of the five normal ventricles were reported.

The shape-volume based validation procedure is easy to implement without the use of extra scanning operation or higher computational cost, yet provides a great way to compare the predication of FE modelling. As tag-MRI is not a routine clinical practice in majority of the hospitals, cine MRI could be used to calculate strain. Cine images are 2D, and thus, out of plane motion cannot be easily estimated (Gao et al., 2015). In addition, due to lack of patterns/features in cine images, higher uncertainties presents while estimating pixel-wise

strain. Gao et al. (2014) showed that the regional circumferential strains could be estimated correctly from cine images. However, greater discrepancies exists during the estimation of regional radial strains, and therefore, could not be used in FE modelling (Gao et al., 2015). Even with tag-MRI, the radial strain cannot be measured with adequate accuracy (Declerck et al., 2000, Denney et al., 2003, Sun et al., 2009). Therefore, when short axis images are used, only single parameter (circumferential strain) could be used for validation which is not sufficient to compare the global deformed shape. Also, it is difficult to estimate strain in late diastole due to the fading of tag data (Gao et al., 2014, Xu et al., 2010) (however, DENSE MRI does not have this issue). It leads to complex and additional computational time. In addition, some studies used (Genet et al., 2014, Gao et al., 2015, Sun et al., 2009) tag MRI in FE modelling without considering the longitudinal basal movement. However, it is evident from the present study that the inclusion of base movement is mandatory for better model prediction. Therefore, shape-volume based validation should be performed along with strain-based validation for improved model prediction.

4.2 Effect of Base Movement

The EDPVRs of LV did not alter due to the inclusion of longitudinal base movement, and therefore, same subject-specific EDV was achieved for both the cases. However, it was observed that the shape-volume prediction was better ($85.91 \pm 2.84\%$ compared to $70.72 \pm 4.05\%$) when longitudinal movement of base was included in the model. It showed that the LV wall expanded more in the radial direction in the fixed base case, and consequently led to inaccurate shape. In addition, including base movement increased the average fibre strain in the LV. These observations indicated two aspects which should be incorporated in any future computational studies of cardiac mechanics. Firstly, the longitudinal base movement should be included in the model; otherwise the model would provide accurate volume estimation with inaccurate geometrical shape. Any surgical

simulations with such inconsistency could result in imprecise model prediction, and therefore, lead to the selection of wrong surgical treatment. Secondly, the traditional method of validating the diastolic model prediction only by comparing the LV EDV (Genet et al., 2014, Lee et al., 2013a), would not be sufficient. Future studies should also compare the geometrical shape to provide precise model estimation for diastole and systole.

4.3 Stress-strain amongst the different wall locations and regions of five ventricles

It was identified that the endocardium region experienced higher fibre stress compared to the epicardium of LV wall at ED. Similar observation was identified by Genet et al. (2014) using scaled myocardium properties for human LV, and by Wenk et al. (2013b) using animal myocardium properties and different constitutive law (fung-type law). Genet et al. (2014) reported that the volume-averaged fibre stress at ED was $2.21 \pm 0.58\ kPa$. In the present study, it was identified that the average fibre stress was in the range of 2 to $3.5\ kPa$ (Figure 6b). Due to the lack of diastolic strain measurement for human myocardium, the circumferential and radial strain values in the present study were compared with the strain values provided for animal heart in the literature. It was reported that the circumferential strain for animal heart was 0.07 to 0.15 (Sinusas et al., 2001), 0.07 to 0.22 (Veress et al., 2005), 0.09 to 0.15 (Guccione et al., 1991) and 0.05 to 0.22 (Omens et al., 1991). In this study, the circumferential strain was in the range of 0.1 to 0.3 (from apex to base), which agreed excellently with the literature. In addition, radial strain for animal heart was reported as 0.15 to 0.25 (Sinusas et al., 2001), 0.09 to 0.14 (Veress et al., 2005), 0.19 to 0.34 (Guccione et al., 1991) and 0.12 to 0.18 (Omens et al., 1991). The absolute value of radial strain was also in the similar range (0.1 to 0.2). Due to the lack of published data on transmural stress-strain distributions in the human LV at ED where human myocardial properties were used (see Table 1), and given the differences in subjects, more detailed

quantitative comparisons do not seem merited. Although the average fibre stress was comparatively higher in the equatorial location, the differences were not considerable. Furthermore, the sheet and sheet-normal stresses and circumferential strain were higher in the basal location compared to the equatorial and the apical locations. Therefore, it was concluded that the LV wall near base location experienced higher stress-strain. In addition, it was observed that the lateral region of LV wall experienced higher fibre and sheet stress. These results were mostly consistent for all five normal human ventricles.

4.4 Limitations and Future Work

First of all, rule-based fibre-sheet orientation was used instead of subject-specific ones. Precise fibre-sheet orientation can be measured only ex-vivo and feasibility of in-vivo diffusion tensor imaging (DTI) for subject-specific fibre-sheet orientation is still an open question (Wang et al., 2009, Genet et al., 2014). The LV EDP was considered 10 *mmHg* due to the unavailability of subject-specific EDP, which requires invasive measurements. Due to such ethical and technical limitations, studies of human ventricular mechanics assumed physiologically reasonable values of ventricular pressure in computational model (Genet et al., 2014, Wang et al., 2013, Lee et al., 2013b, Lee et al., 2013a). The third limitation was the assumption of an initial stress-free state, which was present in all the previous simulations study (Usyk et al., 2000, Genet et al., 2014, Palit et al., 2015b, Sun et al., 2009, Wenk et al., 2011b, Wenk et al., 2011a). Wang et al. (2014) reported that the effects of such initial (residual) stresses are relatively small in late diastole when pressure is higher. In contrast, a recent study observed measurable effect of pre-stress during diastole (Genet et al., 2015). Therefore, it is still an open question and future studies will be carried out to compute personalised diastolic mechanics by considering physiological pre-stress condition.

From the perspective of myocardial physiology and ventricular blood pressure, the structure-functional relations of normal human heart are very complex. It was not claimed that the computational model of BV being able to realistically simulate all the coupled phenomena with inadequate clinical data. However, the model realistically simulated only a limited scope of local LV diastolic mechanics, and within that scope, the model was state-of-the-art in their pragmatism and consistent with which they were validated.

5. Conclusions

In the present study, personalised passive diastolic modelling of human LV was carried out to identify the changes in regional stress-strain distributions in LV wall at ED due to geometrical heterogeneity and base movement. The improvements of the current study over the state-of-the-art as follows. (1) Subject-specific passive orthotropic material properties of human myocardium was used for better model prediction, instead of previously used animal myocardium data with transversely isotropic properties. (2) Personalised computational models of five healthy human ventricles were carried out instead of using single human heart. (3) A new shape-volume based validation procedure was introduced along with traditionally used EDV based comparison. (4) Subject-specific base movement, which was not considered by the majority of previous studies, was included, and consequently, the effect of such movement on model prediction was explored. (5) Bi-ventricular model was considered to include RV deformation. Results indicated that only EDV based validation was not sufficient for accurate model prediction, and therefore, shape-volume relevancy should be compared. Including base movement increased the shape-volume relevancy of LV cavities, and consequently, improved the model prediction. The endocardium of LV wall was experienced high fibre stress compared to the epicardium wall. The LV wall near base location was experienced greater stress and strain compared to the

other locations. In general, the lateral LV wall experienced higher stress-strains compared to the other three regions. In addition, a detailed measurement of different stress-strain components amongst different locations and regions of LV wall was reported for five healthy ventricles. These could be used as a reference map for future computational studies or could serve as targets for in-silico design of therapeutic interventions for diastolic heart failure treatments.

Conflict of interest statement

The authors have no conflict of interest.

Acknowledgements

Financial support was provided by WMG, The University of Warwick. Special mention goes to Dr Sarah Wayte, and Dr Andrew Bell for their valuable suggestions in the work.

Reference:

Arts, T., Costa, K. D., Covell, J. W.,McCulloch, A. D., 2001. Relating Myocardial Laminar Architecture to Shear Strain and Muscle Fiber Orientation. American Journal of Physiology Heart Circulatory Physiology 280.H2222-H2229.

Baillargeon, B., Rebelo, N., Fox, D. D., Taylor, R. L.,Kuhl, E., 2014. The Living Heart Project: A Robust and Integrative Simulator for Human Heart Function. Eur J Mech A Solids 48.38-47.

Costa, K. D., Holmes, J. W.,McCulloch, A. D., 2001. Modelling Cardiac Mechanical Properties in Three Dimensions. The Royal Society 359.1233-1250.

Costa, K. D., Hunter, P. J., Rogers, J. M., Guccione, J. M., Waldman, L. K.,McCulloch, A. D., 1996. A Three-Dimensional Finite Element Method for Large Elastic Deformations of Ventricular Myocardium: I—Cylindrical and Spherical Polar Coordinates. J Biomech Eng 118.452-463.

Declerck, J., Denney, T. S., Öztürk, C., O'Dell, W.,McVeigh, E. R., 2000. Left Ventricular Motion Reconstruction from Planar Tagged Mr Images: A Comparison. Phys Med Biol 45.1611-1632.

Denney, T. S., Jr., Gerber, B. L.,Yan, L., 2003. Unsupervised Reconstruction of a Three-Dimensional Left Ventricular Strain from Parallel Tagged Cardiac Images. Magnetic Resonance in Medicine 49.743-54.

Dokos, S., Smaill, B. H., Young, A. A.,LeGrice, I. J., 2002. Shear Properties of Passive Ventricular Myocardium. American Journal of Physiology Heart Circulatory Physiology 283.H2650-H2659.

Dorri, F., 2004. A Finite Element Model of the Human Left Ventricular Systole, Taking into Account the Fibre Orientation Pattern. PhD. thesis, Swiss Federal Institute Of Technology, Zurich.

Eriksson, T., Prassl, A., Plank, G.,Holzapfel, G., 2013. Influence of Myocardial Fiber/Sheet Orientations on Left Ventricular Mechanical Contraction. Mathematics and Mechanics of Solids 18.592-606.

Fomovsky, G. M., Clark, S. A., Parker, K. M., Ailawadi, G.,Holmes, J. W., 2012. Anisotropic Reinforcement of Acute Anteroapical Infarcts Improves Pump Function. Circulation: Heart Failure 5.515-522.

Gao, H., Allan, A., McComb, C., Luo, X.,Berry, C., 2014. Left Ventricular Strain and Its Pattern Estimated from Cine Cmr and Validation with Dense. Phys Med Biol 59.3637-56.

Gao, H., Li, W. G., Cai, L., Berry, C.,Luo, X. Y., 2015. Parameter Estimation in a Holzapfel–Ogden Law for Healthy Myocardium. Journal of Engineering Mathematics.1-18.

Genet, M., Lee, L. C., Nguyen, R., Haraldsson, H., Acevedo-Bolton, G., Zhang, Z., Ge, L., Ordovas, K., Kozerke, S.,Guccione, J. M., 2014. Distribution of Normal Human Left Ventricular Myofiber Stress at End Diastole and End Systole: A Target for in Silico Design of Heart Failure Treatments. Journal of Applied Physiology 117.142-152.

Genet, M., Rausch, M. K., Lee, L. C., Choy, S., Zhao, X., Kassab, G. S., Kozerke, S., Guccione, J. M.,Kuhl, E., 2015. Heterogeneous Growth-Induced Prestrain in the Heart. Journal of Biomechanics 48.2080-2089.

Göktepe, S., Acharya, S. N. S., Wong, J.,Kuhl, E., 2011. Computational Modeling of Passive Myocardium. International Journal for Numerical Methods in Biomedical Engineering 27.1-12.

Guccione, J. M., Costa, K. D.,McCulloch, A. D., 1995. Finite Element Stress Analysis of Left Ventricular Mechanics in the Beating Dog Heart. Journal of Biomechanics 28.1167-1177.

Guccione, J. M., McCulloch, A. D.,Waldman, L. K., 1991. Passive Material Properties of Intact Ventricular Myocardium Determined from a Cylindrical Model. J Biomech Eng 113.42-55.

Gultekin, O., Sommer, G.,Holzapfel, G. A., 2016. An Orthotropic Viscoelastic Model for the Passive Myocardium: Continuum Basis and Numerical Treatment. Comput Methods Biomech Biomed Engin 19.1647-64.

Holzapfel, G. A.,Ogden, R. W., 2009. Constitutive Modelling of Passive Myocardium: A Structurally Based Framework for Material Characterization. Philosophical Transactions of the Royal Society A 367.3445-3475.

Lee, L., Ge, L., Zhang, Z., Pease, M., Nikolic, S., Mishra, R., Ratcliffe, M.,Guccione, J., 2014. Patient-Specific Finite Element Modeling of the Cardiokinetix Parachute® Device: Effects on Left Ventricular Wall Stress and Function. Medical & Biological Engineering & Computing 52.557-566.

Lee, L. C., Wall, S. T., Klepach, D., Ge, L., Zhang, Z., Lee, R. J., Hinson, A., Gorman, J. H., 3rd, Gorman, R. C.,Guccione, J. M., 2013a. Algisyl-Lvr with Coronary Artery Bypass Grafting Reduces Left Ventricular Wall Stress and Improves Function in the Failing Human Heart. Int J Cardiol 168.2022-8.

Lee, L. C., Wenk, J. F., Zhong, L., Klepach, D., Zhang, Z., Ge, L., Ratcliffe, M. B., Zohdi, T. I., Hsu, E., Navia, J. L., Kassab, G. S.,Guccione, J. M., 2013b. Analysis of Patient-Specific Surgical Ventricular Restoration: Importance of an Ellipsoidal Left Ventricular Geometry for Diastolic and Systolic Function. Journal of Applied Physiology (1985) 115.136-44.

Omens, J. H., May, K. D.,McCulloch, A. D., 1991. Transmural Distribution of Three-Dimensional Strain in the Isolated Arrested Canine Left Ventricle. American Journal of Physiology - Heart and Circulatory Physiolgy 261.H918-H928.

Palit, A., 2015. Computational Modelling of Diastole for Human Ventricle. PhD. thesis, University of Warwick.

Palit, A., Bhudia, S. K., Arvanitis, T. N., Sherwood, V., Wayte, S., Turley, G. A.,Williams, M. A., 2015a. Effect of Fibre Orientation on Diastolic Mechanics of Human Ventricle. Conf Proc IEEE Eng Med Biol Soc 2015.6523-6.

Palit, A., Bhudia, S. K., Arvanitis, T. N., Turley, G. A.,Williams, M. A., 2015b. Computational Modelling of Left-Ventricular Diastolic Mechanics: Effect of Fibre Orientation and Right-Ventricle Topology. Journal of Biomechanics 48.604-612.

Palit, A., Turley, G. A., Bhudia, S. K., Wellings, R.,Williams, M. A., 2014. Assigning Myocardial Fibre Orientation to a Computational Biventricular Human Heart Model. The 15th International Conference on Biomedical Engineering. 2014/01/01. Springer International Publishing, pp. 144-147.

Rohmer, D., Sitek, A.,Gullberg, G. T., 2007. Reconstruction and Visualization of Fiber and Laminar Structure in the Normal Human Heart from Ex Vivo Diffusion Tensor Magnetic Resonance Imaging (Dtmri) Data. Investigative Radiology 42.777-789.

Sinusas, A. J., Papademetris, X., Constable, R. T., Dione, D. P., Slade, M. D., Shi, P.,Duncan, J. S., 2001. Quantification of 3-D Regional Myocardial Deformation: Shape-Based Analysis of Magnetic Resonance Images. Am J Physiol Heart Circ Physiol 281.H698-714.

462 Sommer, G., Haspinger, D., Andra, M., Sacherer, M., Viertler, C., Regitnig, P.,Holzapfel, G. A.,
463 2015a. Quantification of Shear Deformations and Corresponding Stresses in the Biaxially
464 Tested Human Myocardium. Annals of Biomedical Engineering 43.2334-2348.
465 Sommer, G., Schriefl, A. J., Andrä, M., Sacherer, M., Viertler, C., Wolinski, H.,Holzapfel, G. A.,
466 2015b. Biomechanical Properties and Microstructure of Human Ventricular Myocardium.
467 Acta Biomaterialia 24.172-192.
468 Stevens, C., Remme, E., LeGrice, I.,Hunter, P., 2003. Ventricular Mechanics in Diastole: Material
469 Parameter Sensitivity. Journal of Biomechanics 36.737-748.
470 Streeter, D. D. J., Spotnitz, D. P. P., Ross, J. J.,Sonnenblick, E. H., 1969. Fiber Orientation in the
471 Canine Left Ventricle During Diastole and Systole. Circulation Research 24.339-347.
472 Sun, K., Stander, N., Jhun, C.-S., Zhang, Z., Suzuki, T., Wang, G.-Y., Saeed, M., Wallace, A. W.,
473 Tseng, E. E., J.Baker, A., Saloner, D., Einstein, D. R., Ratcliffe, M. B.,M.Guccione, J., 2009.
474 A Computationally Efficient Formal Optimization of Regional Myocardial Contractility in a
475 Sheep with Left Ventricular Aneurysm. J Biomech Eng 131.111001/1 - 111001/10.
476 Usyk, T. P., Mazhari, R.,McCulloch, A. D., 2000. Effect of Laminar Orthotropic Myofiber
477 Architecture on Regional Stress and Strain in the Canine Left Ventricle. Journal of Elasticity
478 31.143-164.
479 Veress, A. I., Gullberg, G. T.,Weiss, J. A., 2005. Measurement of Strain in the Left Ventricle During
480 Diastole with Cine-Mri and Deformable Image Registration. J Biomech Eng 127.1195-207.
481 Vetter, F. J.,McCulloch, A. D., 2000. Three-Dimensional Stress and Strain in Passive Rabbit Left
482 Ventricle: A Model Study. Annals of Biomedical Engineering 28.781 - 792.
483 Walker, J. C., Ratcliffe, M. B., Zhang, P., Wallace, A. W., Hsu, E. W., Saloner, D. A.,Guccione, J.
484 M., 2008. Magnetic Resonance Imaging-Based Finite Element Stress Analysis after Linear
485 Repair of Left Ventricular Aneurysm. The Journal of Thoracic and Cardiovascular Surgery
486 135.1094 - 1102.
487 Wall, S. T., Walker, J. C., Healy, K. E., Ratcliffe, M. B.,Guccione, J. M., 2006. Theoretical Impact of
488 the Injection of Material into the Myocardium: A Finite Element Model Simulation.
489 Circulation 114.2627-35.
490 Wang, H. M., Gao, H., Luo, X. Y., Berry, C., Griffith, B. E., Ogden, R. W.,1, T. J. W., 2013.
491 Structure-Based Finite Strain Modelling of the Human Left Ventricle in Diastole.
492 International Journal for Numerical Methods in Biomedical Engineering 29.83-103.
493 Wang, H. M., Luo, X. Y., Gao, H., Ogden, R. W., Griffith, B. E., Berry, C.,Wang, T. J., 2014. A
494 Modified Holzapfel-Ogden Law for a Residually Stressed Finite Strain Model of the Human
495 Left Ventricle in Diastole. Biomech Model Mechanobiol 13.99-113.
496 Wang, J.,Nagueh, S. F., 2009. Current Perspectives on Cardiac Function in Patients with Diastolic
497 Heart Failure. Circulation 119.1146-1157.
498 Wang, V. Y., Lam, H. I., Ennis, D. B., Cowan, B. R., Young, A. A.,Nash, M. P., 2009. Modelling
499 Passive Diastolic Mechanics with Quantitative Mri of Cardiac Structure and Function.
500 Medical Image Analysis 13.773-784.
501 Wenk, J. F., Eslami, P., Zhang, Z., Xu, C., Kuhl, E., III, J. H. G., Robb, J. D., Ratcliffe, M. B., MD, R.
502 C. G.,Guccione, J. M., 2011a. A Novel Method for Quantifying the in-Vivo Mechanical
503 Effect of Material Injected into a Myocardial Infarction. Ann Thorac Surg 92.935 - 941.
504 Wenk, J. F., Ge, L., Zhang, Z., Mojsejenko, D., Potter, D. D., Tseng, E. E., Guccione, J. M.,Ratcliffe,
505 M. B., 2013a. Biventricular Finite Element Modeling of the Acorn Corcap Cardiac Support
506 Device on a Failing Heart. Ann Thorac Surg 95.2022-7.
507 Wenk, J. F., Ge, L., Zhang, Z., Soleimani, M., Potter, D. D., Wallace, A. W., Tseng, E., Ratcliffe, M.
508 B.,Guccione, J. M., 2013b. A Coupled Biventricular Finite Element and Lumped-Parameter
509 Circulatory System Model of Heart Failure. Comput Methods Biomech Biomed Engin
510 16.807-18.
511 Wenk, J. F., Sun, K., Zhang, Z., Soleimani, M., Ge, L., Saloner, D., Wallace, A. W., Ratcliffe, M.
512 B.,Guccione, J. M., 2011b. Regional Left Ventricular Myocardial Contractility and Stress in a
513 Finite Element Model of Posterobasal Myocardial Infarction. J Biomech Eng 133.044501-1 -
514 044501-6.
515 Wong, J.,Kuhl, E., 2014. Generating Fibre Orientation Maps in Human Heart Models Using Poisson
516 Interpolation. Computer Methods in Biomechanics and Biomedical Engineering 17.1217-26.

517 Xu, C., Pilla, J. J., Isaac, G., Gorman, J. H., Blom, A. S., Gorman, R. C., Ling, Z.,Dougherty, L.,
518 2010. Deformation Analysis of 3d Tagged Cardiac Images Using an Optical Flow Method.
519 Journal of Cardiovascular Magnetic Resonance 12.1-14.

520

Caption of the figures:

Figure 1: Subject-specific values. (a) Early Diastolic Volume (ErDV), End Diastolic Volume (EDV) and Ejection Fraction (EF) extracted from CMRI of five normal ventricles (BV1 to BV5); (b) Measurement procedure of longitudinal base and apex movement ; (c) Longitudinal movement of base and apex measured for five ventricles (BV1 to BV5)

Figure 2: (a) Subject-specific bi-ventricular mesh geometry; (b) LV cavity at early diastole constructed from cardiac MRI; (c) LV cavity at end diastole constructed from cardiac MRI; (d) fibre orientation map using LDRF algorithm

Figure 3: Effect of base movement on diastolic model prediction. (a) EDPVRs of LV for both cases (i.e. base fix vs base move) show that the EDPVR remains same even with the inclusion of base movement; (b) Procedure to calculate intersected volume to incorporate the shape-volume relevancy at ED; (c) Percentage of intersected volume between original and simulated LV cavity at ED; it shows that the better model prediction is achieved when base movement is included

Figure 4: Comparison between fibre stress (Cauchy) and fibre strain (logarithmic) predictions between the two cases (base move vs base fix) for BV1. The location definition of the images are described in section 2.4

Figure 5: Subject-specific fibre stress (Cauchy stress) at three short axis (base, equatorial and apex) and two long-axis (s-l and a-p) locations. The location definition of the images are described in section 2.4

Figure 6 : (a) Range and (b) average values of the fibre (ff), sheet (ss) and sheet-normal (nn) stresses at base, equatorial and apical locations of each BV; (c) Range and (b) average values of the circumferencial (cc), longitudinal (ll) and radial (rr) strains at base, equatorial and apical locations of each BV.

Figure 7: (a) Range and (b) average values of the fibre (ff), sheet (ss) and sheet-normal (nn) stresses at anterior (A), lateral (L), posterior (P) and septum (S) regions of each locations (i.e. base, equatorial and apical) of each BV

Figure 8 : (a) Range and (b) only average values of the circumferencial (cc), longitudinal (ll) and radial (rr) strains at anterior (A), Lateral (L), posterior (P) and septum (S) regions of each location (i.e. base, equatorial and apical) of each BV.

Figure 1

Click here to download high resolution image

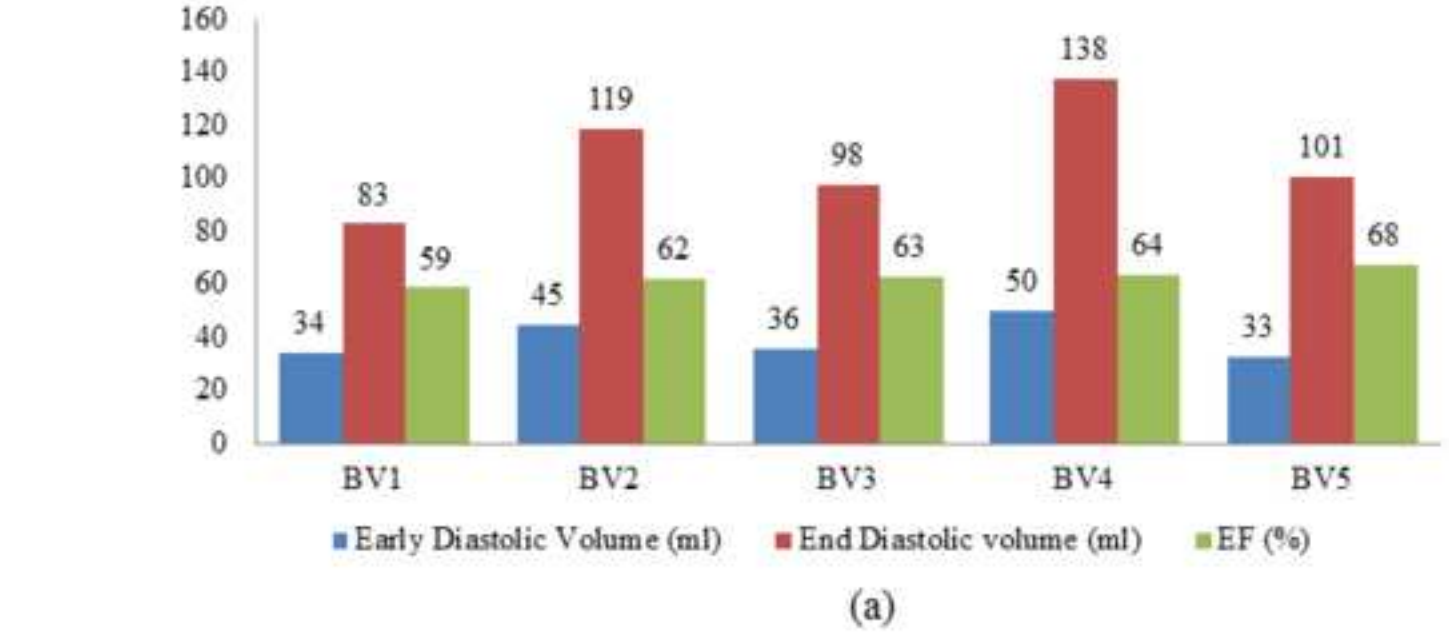

(a)

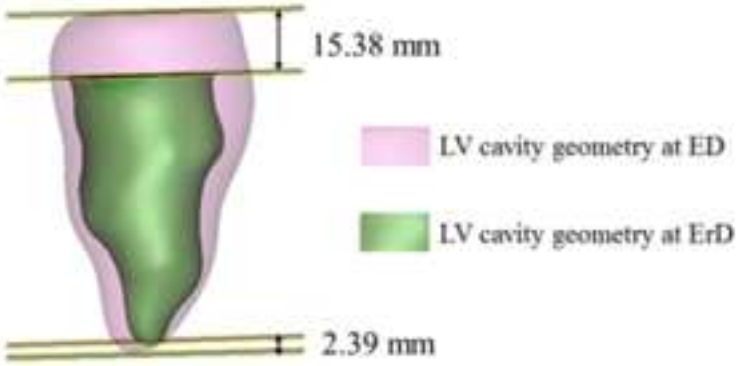

(b)

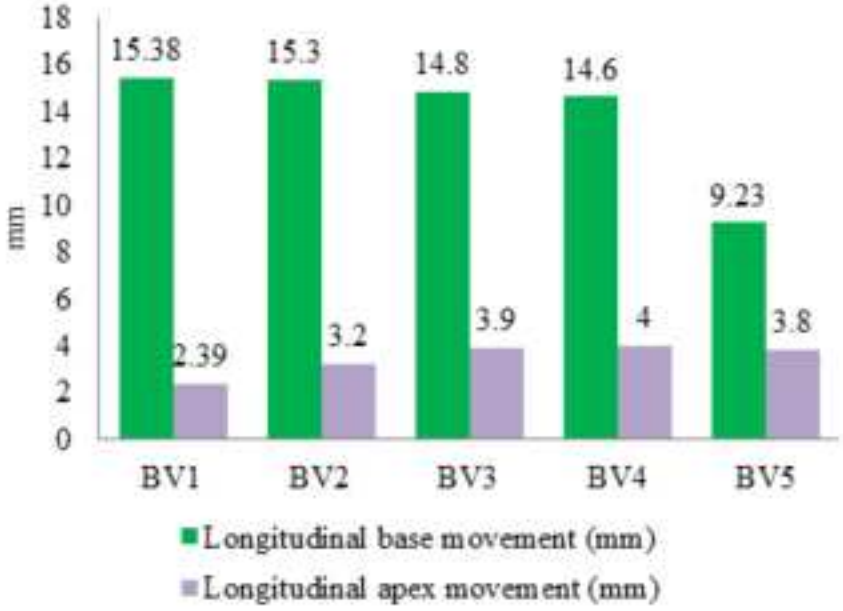

(c)

Figure 2

Click here to download high resolution image

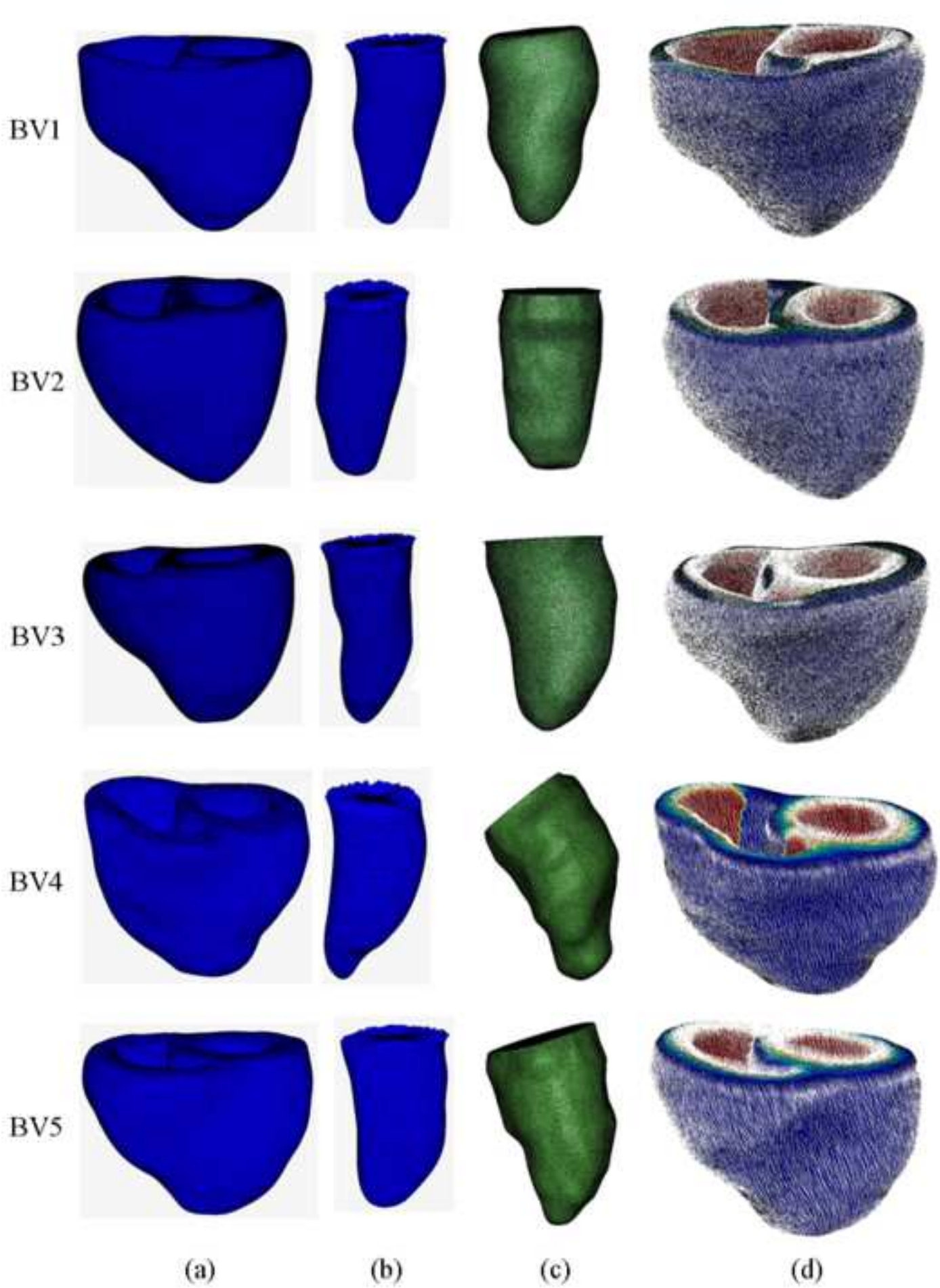

Figure 3

Click here to download high resolution image

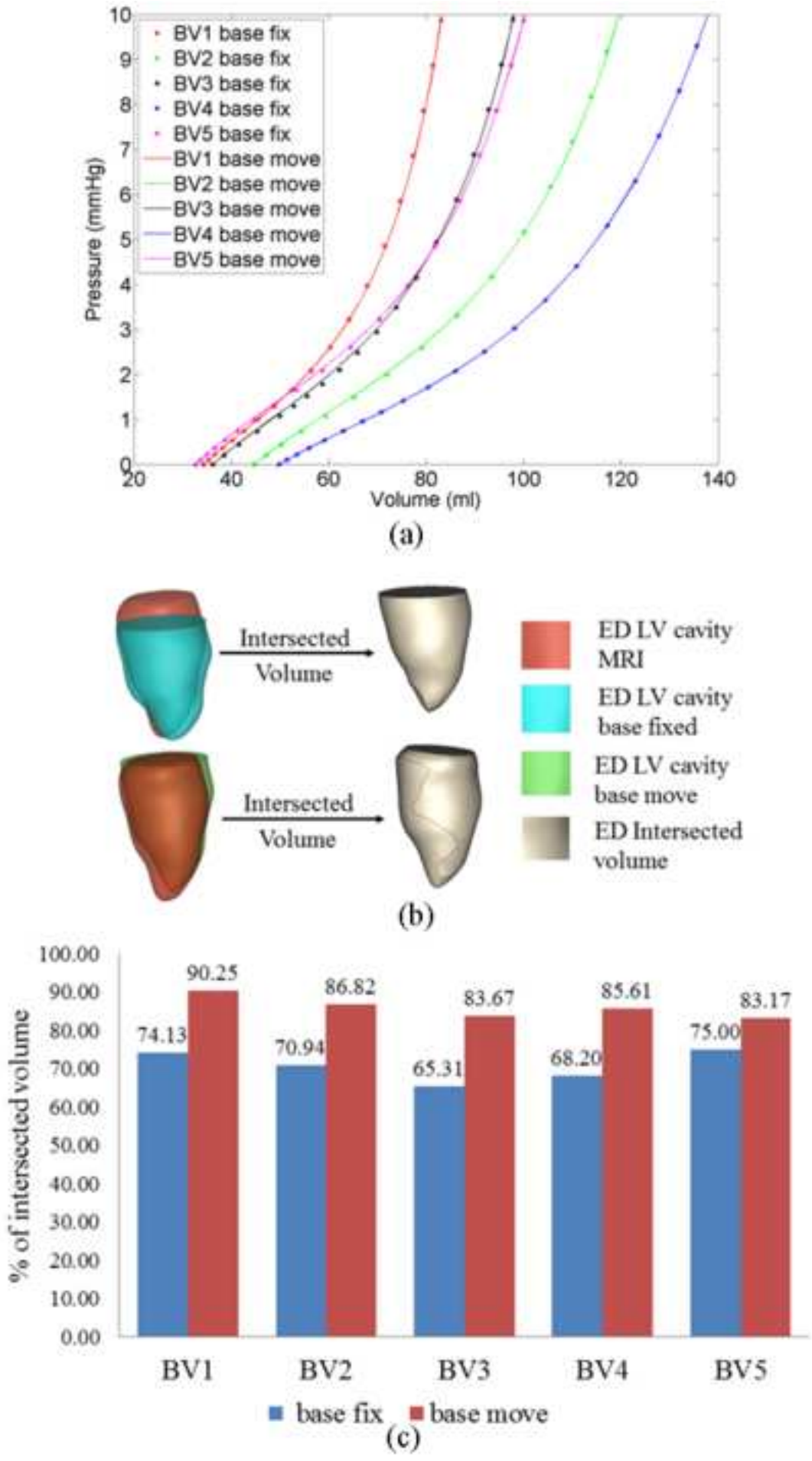

Figure 4

Click here to download high resolution image

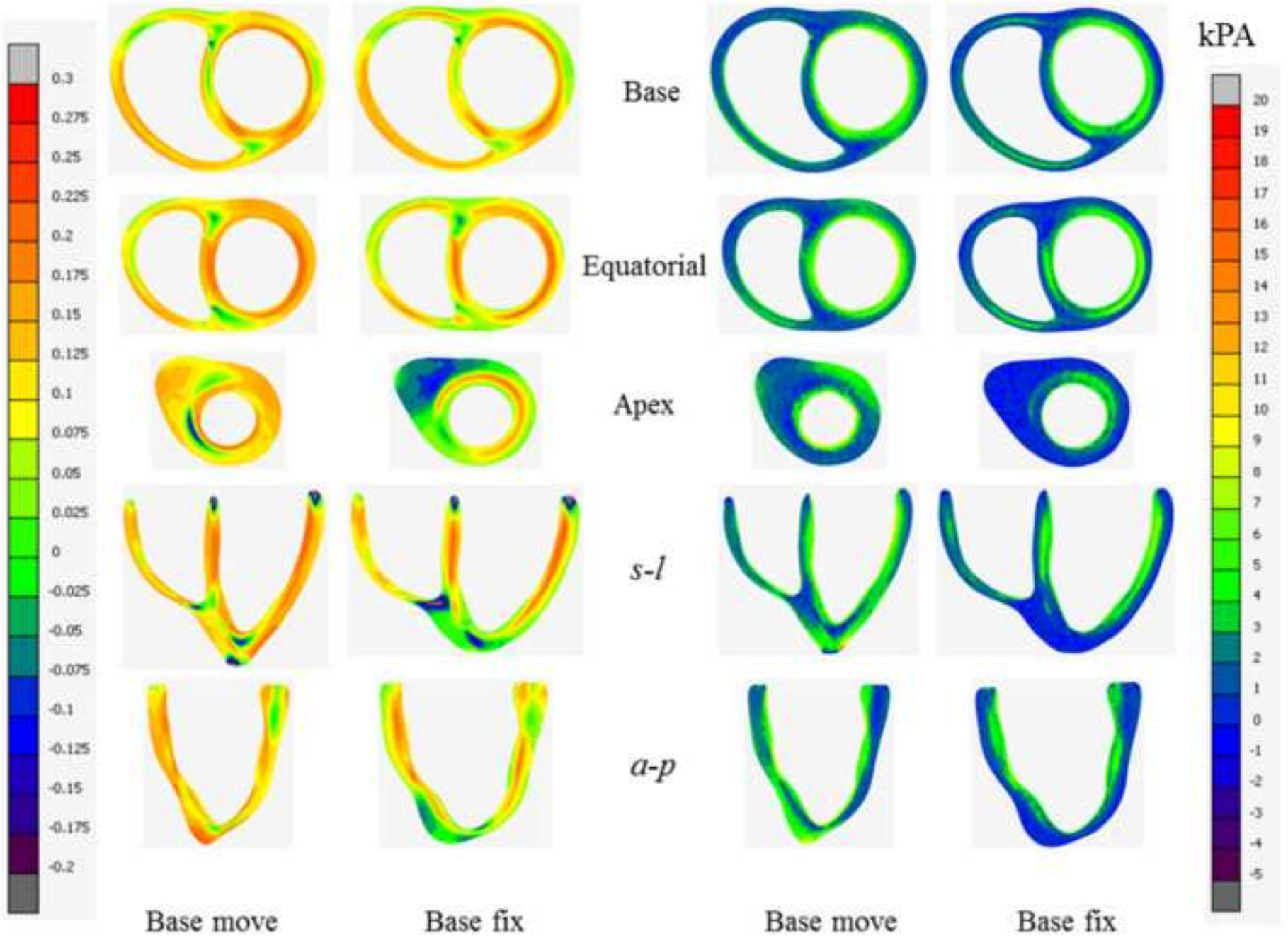

Figure 5

Click here to download high resolution image

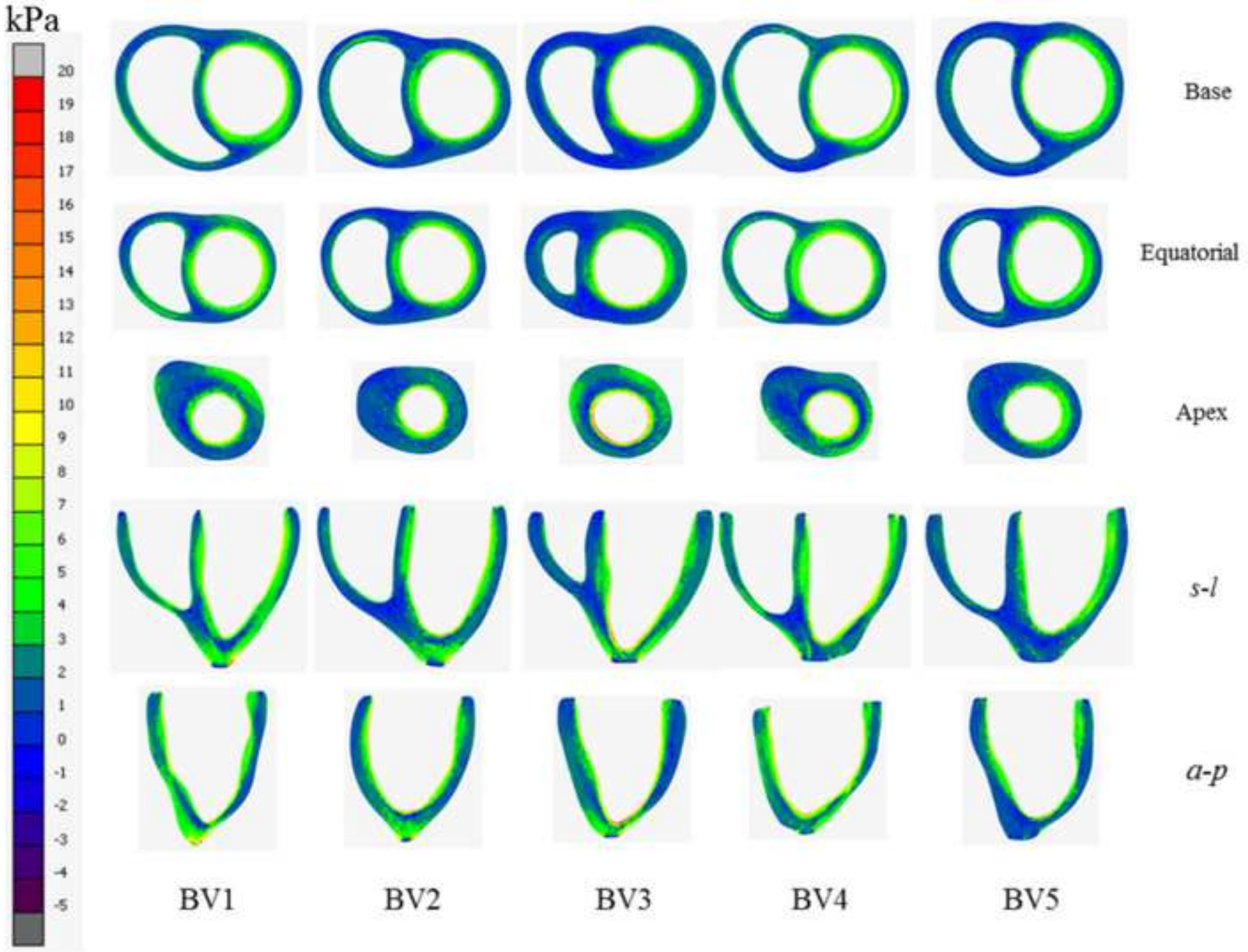

Figure 6

Click here to download high resolution image

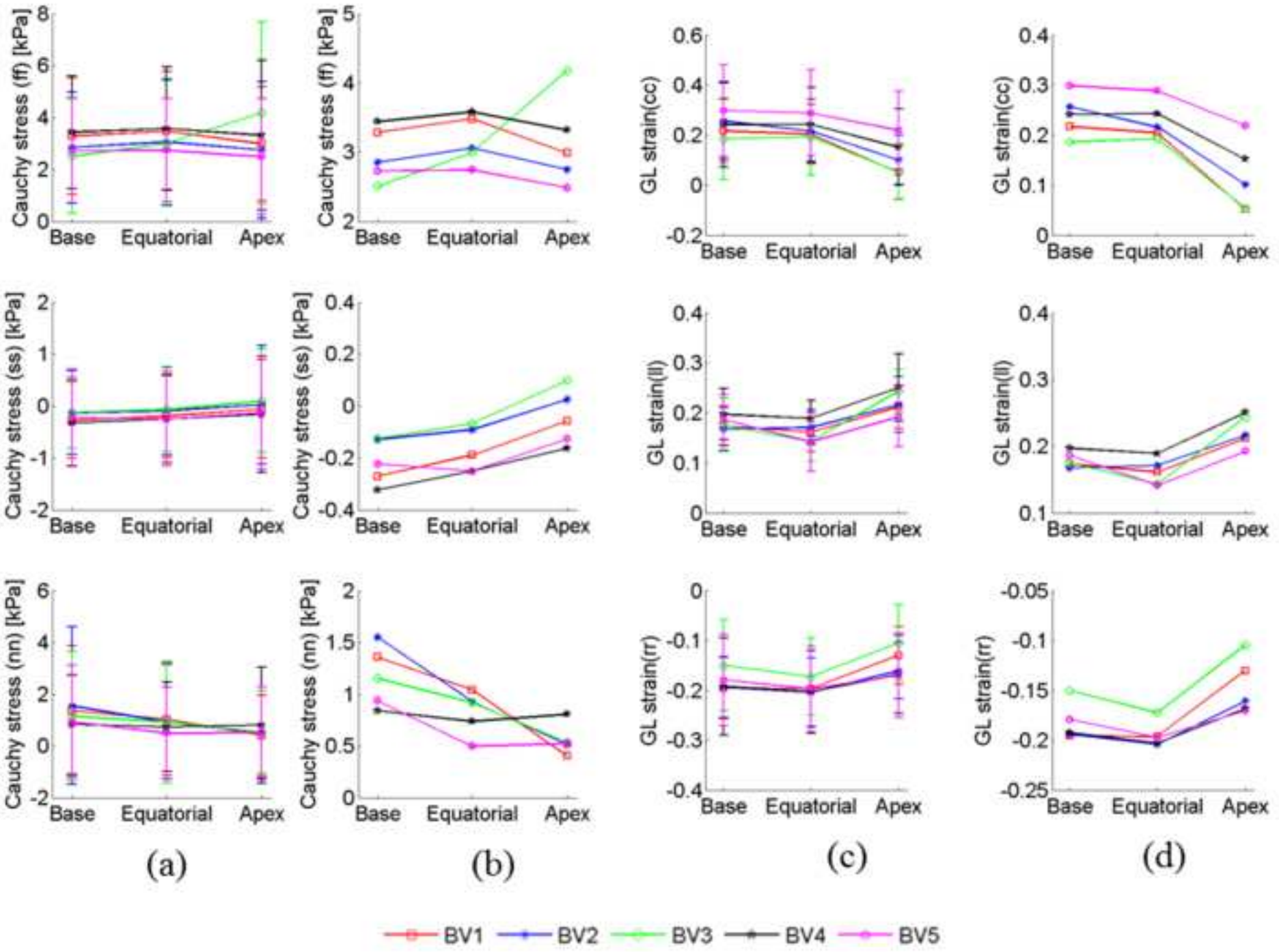

Figure 7

Click here to download high resolution image

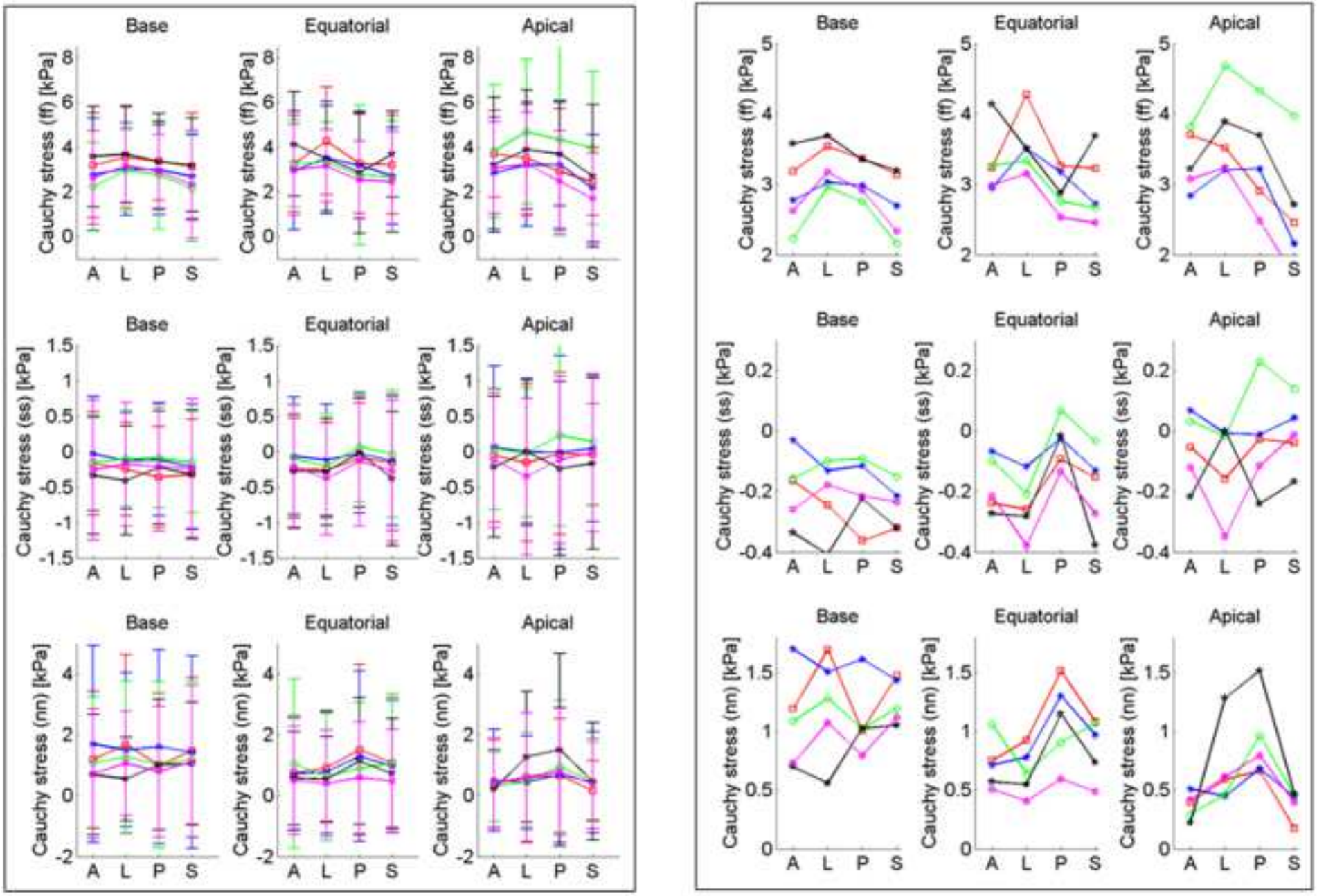

Figure 8

Click here to download high resolution image

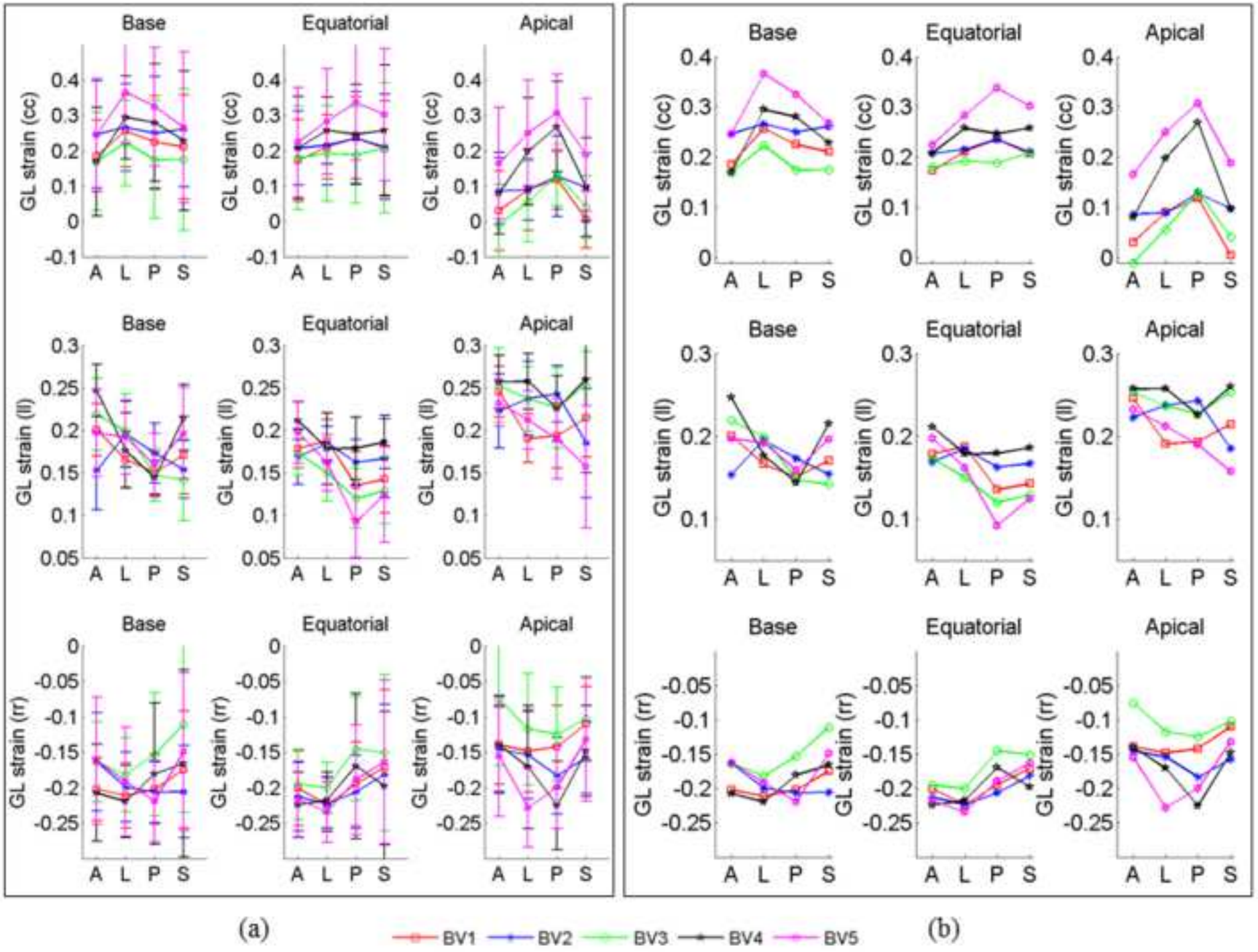

Table 1

Table 1: Previous work on passive diastolic modelling of LV with the key attributes considered in the study

	Single LV		Bi-ventricle (BV)		Effect of base movement
	Animal myocardium passive properties	Human myocardium passive properties	Animal myocardium passive properties	Human myocardium passive properties	
Animal ventricle / Idealised geometry	Humphrey and Yin (1989) Guccione et al. (1995) Costa et al. (1996) Vetter and McCulloch (2000) Usyk et al. (2000) Wang et al. (2009)	-	Stevens et al. (2003)	-	-
Transversely isotropic	Humphrey and Yin (1989) Guccione et al. (1995) Costa et al. (1996) Vetter and McCulloch (2000) Wang et al. (2009)	Genet et al. (2014)	-	-	-
Human ventricle	Wang et al. (2013)	Genet et al. (2014)	Palit et al. (2015)	Research in this paper	
Orthotropic	Usyk et al. (2000) Wang et al. (2013)	-	Stevens et al. (2003) Palit et al. (2015) Göktepe et al. (2011)		
Effect of global Geometric Heterogeneity	-	Genet et al. (2014)	-		

Table 2

Table 2: Subject-specific values of Holzapfel-Ogden material parameters used in this study

Subject	Passive Material Properties							
	a (kPa)	b	a_f (kPa)	b_f	a_s (kPa)	b_s	a_{fs} (kPa)	b_{fs}
BV1	0.080	6.00	2.951	5.893	0.492	3.393	0.070	3.929
BV2	0.092	4.800	2.647	5.323	0.441	3.065	0.063	3.548
BV3	0.089	4.760	2.579	5.000	0.430	2.879	0.061	3.333
BV4	0.060	4.450	2.500	4.853	0.417	2.794	0.059	3.235
BV5	0.048	4.380	2.466	5.000	0.411	2.879	0.058	3.333